A framework for estimating unresolved spectral shade

Alan R. Gillespie[1*], Laura Gilson[1], Michael A. O'Neal[2] and Van R. Kane[3]
[1)] Department of Earth and Space Sciences, University of Washington, Seattle, WA 98195 USA
[2)] Department of Geography, University of Delaware, Newark, DE 19716 USA
[3)] College of Forest Resources, University of Washington, Seattle, WA 98195 USA
[*] arg3@u.washington.edu; +1 206 685 8265

ABSTRACT - Spectral Mixture Analysis (SMA) is a standard way of analyzing spectral images in terms of fundamental components of the scene. For images in reflected sunlight, much of the image variance is caused by lighting variations - shadowing and photometric shading - that is accounted for by using a shade endmember located close to the origin in a spectral DN space. Under control of the lighting and viewing geometry, shade mixes with the tangible spectral endmembers such as soil and green vegetation to produce the observed spectral radiances. In many scenes, the landscape is vegetated and shade comprises topographic shading and shadowing ("hillshade"), which results from unresolved shadows cast by the canopy ("treeshade") and shadows cast by elements of the canopy ("leafshade"). Hillshade is commonly estimated using digital elevation models (DEMs) and assuming unvegetated surfaces are Lambertian. Deviations from hillshade include treeshade and leafshade. In general, we use LiDAR DEMs with 1-m resolution to model hillshade ("bare earth" or "last arrival") and treeshade ("first arrival" minus bare earth). In this study of a low-relief forested area in Maryland, USA, we use LiDAR to estimate treeshade and SMA to calculate the shade endmember fractions for an ASTER image of the same area taken near the same time of year (leaf-on). The differences between the LiDAR-based model and the shade image are used to parse shade into its basic constituents and give the first remote-sensing estimates of the relative magnitude of leafshade and treeshade in a forest dominated by deciduous trees.

1 INTRODUCTION

Images of forested landscapes are dominated by the mutual shadowing of trees by their neighbors, and by self-shadowing and scattering from leaves within the canopy. By contrast, spectral shape is similar from stand to stand. A large body of work has been devoted to forward models of the bidirectional reflectance distribution function from canopies in order, ultimately, to account for such effects (e.g., *Verhoef*, 1984; *Franklin et al.*, 1991; *Li et al.*, 1995; *Dymond et al.*, 2001). *Franklin et al.,* (1991) noted the need for improved correction for topographic slopes in forests, leading to the SCS model of *Gu and Gillespie* (1998). As emphasized by *Strahler* (1997), however, the problem of inversion to derive biophysical parameters (*e.g.*, *Hall et al.*, 1997) from spectral images has not been fully solved. The present study is a step in that direction made by associating shade components with the canopy features that create them.

Early in the history of remote sensing, *Kauth and Thomas* (1976) recognized the importance of the "point of all shadows" in their data-invariant "tasseled cap" transformation, designed to associate physical parameters with image channels. *Adams et al.* (1986) improved on the tasseled cap transformation with data-dependent spectral mixture modeling (SMA), in which the "point of all shadows" was re-introduced as "shade," or darkening due to lighting and canopy roughness (i.e., shading and shadowing). In SMA, the corresponding Shade spectral endmember is a radiance vector ("Shade" with a capital refers to the specific image endmember rather than "shade," the physical scene component). However, modeling bare surfaces with the Shade (*Sh*) endmember proved to be simpler than modeling canopies, for which physical shade itself was less well-defined (e.g., *Roberts et al.*, 1993). Low-albedo surfaces also can mimic shadowed ones.

SMA is now a standard processing strategy for multispectral and hyperspectral images (*Sabol et al.*, 2002; *Adams and Gillespie*, 2006). For the inverse model, "unmixing," *Sh* and the other spectral endmembers are expressed as fraction images, in which the contribution of each endmember is represented as a fraction of the total radiance for each pixel. In forested scenes, *Sh* is best regarded as the integrated darkening due to topographic shading ("hillshade") plus resolved and unresolved shadows. It is also related to shading of sunlit leaves. However, it has proven difficult to separate shade into its separate components.

Unresolved shadows in satellite images arise from surface roughness plus trees ("treeshade"), together with shadows cast within the canopy by leaves ("leafshade"). Recent advances in high-resolution LiDAR imaging allow us to independently measure DEMs at the meter scale for the canopy.

From these DEMs, treeshade can be predicted and compared to *Sh* fraction images, with differences attributed to leafshade. Parsing shade into its components is important because it allows us to develop a quantitative assessment for how much darkening is contributed to spectral images from the various sources. The objective of the present study is to split the *Sh* fraction produced in SMA of satellite images into treeshade and leafshade for a low-relief scene with nearly constant topographic effects.

2 BACKGROUND

2.1 Spectral Mixture Analysis (SMA)

SMA is discussed at length in *Adams and Gillespie* (2006). The general equation expressing measured spectral radiances L as linear mixtures of fundamental spectral components is

$$L_j = \sum f_k E_{j,k} + \delta_j \quad m < n+1 \qquad (1)$$

- L_j spectral radiance ($Wm^{-2}\mu m^{-1}sr^{-1}$) in image channel j
- $E_{j,k}$ L vector for spectral endmember k in image channel j
- f_j fraction of spectrum E for endmember k needed to model L_j for a specific pixel
- δ_φ unmodeled residual for channel j
- m number of spectral endmembers
- n number of image channels

Equation 1 is over-determined and may be solved by least-squares methods. Channel residuals δ_j are generally grouped and expressed as a root-mean-squared value, *rms*. For a well-modeled image, *rms* will approach the precision value for the spectral radiance data, usually 1-2 DN. If the set of E is thought to describe all the spectral variance of a scene, the assumption is generally made that

$$\Sigma f_j = 1 \qquad (2)$$

This called the "constrained" model. If an incomplete set of endmembers is desired, an unconstrained model not invoking Equation 2 is used instead, and $m<n$.

Spectral endmembers are commonly picked from images using training areas. Image-defined endmembers are therefore not "pure" and may contain characteristic mixtures of some or all endmembers in the model. In such cases "overflow" fractions ($f<0$ or $f>1$) are common. Such values simply mean that there is more or less of E_k in a pixel than in the region used to define it. It is also possible to pick endmembers from inspection of the spectral radiance cloud in DN space. However they are picked, endmembers should represent physically meaningful scene constituents that commonly mix together, and they must be spectrally distinct. The fraction of Shade, f_{sh}, is temporally variable. For closed-canopy forests, commonly one or two endmembers are needed to account for green vegetation, and another to account for woody material.

2.2 *Shade* fraction (f_{sh})

f_{sh} is influenced by many factors, including resolved and unresolved shadows down-sun from occulting elements of the scene, and shading, or darkening due to geometrically reduced illumination (tilted surfaces). These occur at all scales in the scene, but it is convenient to consider threshold scales at which spectral measurements are made (for ASTER VNIR images, this is 15 m/pixel) and at which shadow measurements are made (e.g., the 1-m spacing of the LiDAR measurements). At the 1-m scale, the shade fraction for low-relief scenes comprises shadows from the canopy and leaves, and the integrated shading of the sunlit canopy due to local leaf incidence angles. It may be described as a product of S and $\Lambda\cdot(1-a\cdot\chi)$ (terms defined below; in the LiDAR data, shadow S is either 0 or 1) but this cannot be simply integrated to the 15-m ASTER scale because cm-scale leafshade Λ is only defined using ASTER ($\int(S\cdot(1-a\cdot\chi)\cdot\Lambda) \neq \int(S\cdot(1-a\cdot\chi))\cdot\int\Lambda$). Thus, an approximation describing f_{sh} in terms of its constituents at the 15-m scale is

$$c_0+c_1 f_{sh} \approx S+(1-S)\,\Lambda+(1-(S+(1-S)\Lambda))\cdot(1-a\chi(i)) \qquad (3)$$

- where $(1-(S+(1-S)\cdot\Lambda))$ is the F_{sh} contributed by unshadowed, sunlit portion of the 15-m pixel and the right-hand side of eqn. 3 excluding the first term, S, is leafshade.
- f_{sh} Shade fraction calculated in SMA. f_{sh} = 1 corresponds to the Shade endmember and f_{sh} = 0 to a mixing line or plane defined by the other endmembers (such as green vegetation and soil).
- c_0, c_1 calibration offset and gain factor. Image-defined endmembers may contain a fraction of shade, but f_{sh} = 0.0 should correspond to zero shade. The Shade endmember itself is defined as 100% shade.
- S treeshade shadow fraction, integrated to the image scale. Shadows unresolved by the LiDAR are included as a component of "leafshade."
- i the solar incidence angle.
- χ integrated reflectance for the sunlit part of the canopy. For diffuse Lambertian surfaces, $\chi = \cos(i)$; for real canopies scattering is not diffuse. For uniform reflectance, $\chi = 1$, independent of i.
- a relative albedo, the change in f_{sh} caused by absorption of light by the surface (*e.g.*, a leaf) relative to the albedo of the tangible endmember. Albedo is a property of composition, not structure.
- Λ leafshade shadow fraction, defined as shadows from unresolved leaves and branches (or by rough surface elements in exposed substrate) integrated to the

image scale. Λ is a property of structure, not composition.

3 APPROACH

We identified a low-relief forested scene for which both ASTER and LiDAR images acquired in late spring were available. The ASTER image was analyzed by conventional SMA; the LiDAR DEM was processed to isolate the canopy, from which treeshade was calculated and used to calibrate the ASTER f_{sh}. Differencing or ratioing f_{sh} and the treeshade image will give an image approximating leafshade (*Retzlaff et al.*, 2002), but we used the more rigorous equation 3. The novel aspects of the approach were combining LiDAR and optical imaging to give a new view of a fundamental remote-sensing property of tree canopies, devising a calibration strategy for f_{sh}, and elaborating the mixing model to provide a framework for this new analysis.

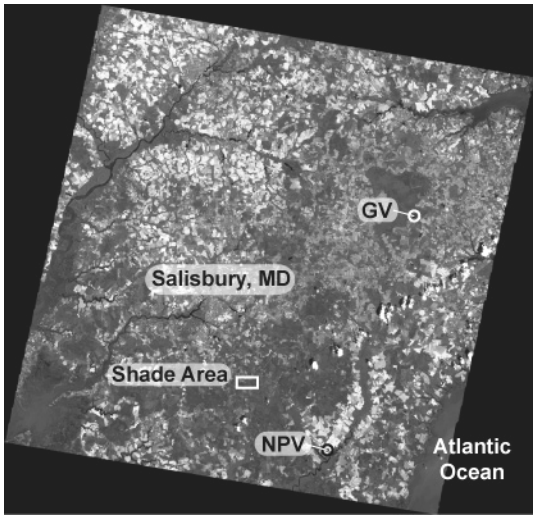

Figure 1. ASTER radiance image including study area, 15 May 2004 (60 km across; north is up). Bare fields are light; forests and wetlands are dark. "Shade Area," GV, and NPV are locations used to select spectral endmember DN vectors; Shade was modified as described in the text.

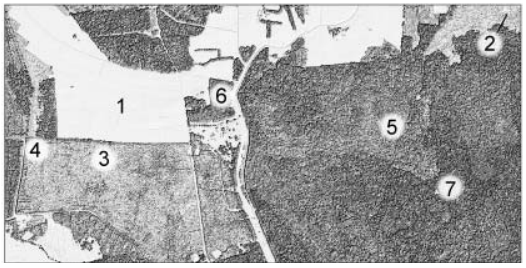

Figure 2. First-arrival 1-m LiDAR shade image, 2.6 km across, complemented so that areas of high treeshade are dark, as would be seen in an air photo. North is up. Numbers indicate cover classes: 1- bare earth and grass (0-1 m), 2 - crops, shrubs, small trees (1-5 m), 3 - forest (5-10 m), 4 - forest (10-15 m), 5 - forest (15-20 m), 6 - forest (20-25 m), 7 - forest (25-30 m).

3.1 Test site

The test site (Fig. 1, 2) is located 12 km SSE of Salisbury, MD (USA) at 38.260ºN, 75.549ºW and 14 m elevation, on Greenbrier Swamp Road (N-S). It is 1.1 km N-S by 2.6 km E-W, and consists of grassy and bare fields and deciduous forests of different ages and structural stages. Total surface relief is <9 m, but forest canopies are as high as 30 m. Stands are dominated by broadleaf trees such as hickory and oak.

3.2 Spectral data and SMA

A largely cloud-free ASTER image (atmospherically compensated, land-leaving spectral radiance: AST09), was selected for SMA (Fig. 1). Three VNIR channels (0.56, 0.66, and 0.81 μm) were analyzed as linear mixtures of Shade (*Sh*), green vegetation (*GV*), and woody material (*NPV*).

The three spectral endmembers were defined from the image near the test site (Fig. 1, Table 1). GV was defined by a stand of light, low-shade deciduous trees. *NPV* was defined by a bare field. *Sh* was approximated by the darkest non-water pixels in the image, but the definition was refined (and DN values lowered) according to the intersection of mixing lines in the data (*DN*) space because the image-defined *Sh* did not lie on the mixing line to NPV. Nevertheless, the *Sh* endmember *DN* values were all well above zero. Non-zero *Sh* values arise due to uncompensated atmospheric path radiance, light scattered into shadows by adjacent scene elements, and/or measurement bias.

ASTER Channel	Sh (DN)	GV (DN)	NPV (DN)
1	51	78	173
2	27	37	146
3	30	134	110

Table 1. Endmember spectra: Green vegetation (GV; non-photosynthetic vegetation (NPV); and Shade (Sh).

3.3 High-resolution measurement of topography

LiDAR images of the test area were from a dataset acquired by the State of Maryland's Department of

Natural Resources between June and July of 2003.[1] First-return LiDAR "point-cloud" postings were <1 m, and vertical resolution was 14.3 cm. At this fine scale, different types of trees may be recognized by shape.

3.4 Calculation of *S*

Canopy shadow and shading images *S* and $S \cdot \chi$ were calculated from the 1st-arrival LiDAR data with ArcInfo and ERDAS Imagine, respectively. The 1st-arrival and canopy DEMs were similar. Last-return data yielded sparse information in homogeneous areas of the topographically subtle terrain and gridded data were created from a triangulated irregular network. Figure 2 shows the full-resolution LiDAR shade image from which 1-m/pixel images of *S* and $S \cdot \chi$ were calculated.

The 1-m LiDAR shade data are at too fine a scale for direct comparison to the 15-m ASTER f_{sh} image. Therefore, they were low-pass filtered with a 15x15 m equal-weight kernel and resampled to 15-m resolution.

3.5 Calibration of f_{sh}

The shade found from SMA is relative to the amount in the image-defined endmembers. Actual shade in the endmembers *GV* and *NPV* may be nonzero and different (Fig. 3). Therefore comparison to LiDAR-derived shade requires calibration, which can be achieved if different areas differ only in their amount of LiDAR-determined *S*. Linear regression of *S* onto f_{sh} yields c_0 directly (the intercept), and the slope is

$$\Delta S/\Delta f_{sh} = c_1/(a \cdot \chi \cdot (1 - \Lambda)) \qquad (4)$$

In this study, observation leads us to estimate that $\chi = 1$, *a* is known and constant, and Λ is unknown but constant among nearby forest stands of units 5-7 (*GV>>NPV*) as defined in Figure 2. Therefore, Eqn 4 contains two unknowns (c_1, Λ) which may be found if two or more pairs of f_{sh} and S have been measured.

Because χ, *a*, and Λ may all differ among tangible endmembers (*i.e.*, excluding *Sh*) a different calibration may be necessary for each endmember (Fig. 3). This reflects the fact that *S* may differ among image-defined tangible endmembers. In this study we calibrated only along the *GV – Sh* mixing line, because roughness in bare fields was < 1 m/pixel so $S = 0$.

3.6 Calculation of leafshade

In calibration, Λ was assumed to be constant for selected stands. In general, however, this assumption may not be true, and the goal of the research was to find leafshade across the image, using Eqn 3 with f_{sh} and *S* as input. Isolating Λ requires that *a* is known, and with the data at hand it can only be estimated: e.g., for deciduous tree leaves, $a \approx 0.23$ according to the ASTER Spectral Library (http://speclib.jpl.nasa.gov). This value is <0.02 greater than for conifer needles, but may be different for *NPV* and soils. In principle, we can measure typical values of *a* for different stands if we know function χ since we can determine *i* from DEMs, but for forest stands we assumed χ=1, recognizing this too as an approximation (*e.g.*, *Li et al.*, 1995). We nevertheless calculated a shading image for χ=cos(i) for comparison with the other derived image products. Although χ can be calculated directly from the LiDAR DEM, we estimated it from the derived shade image, interpolating across areas of shadow.

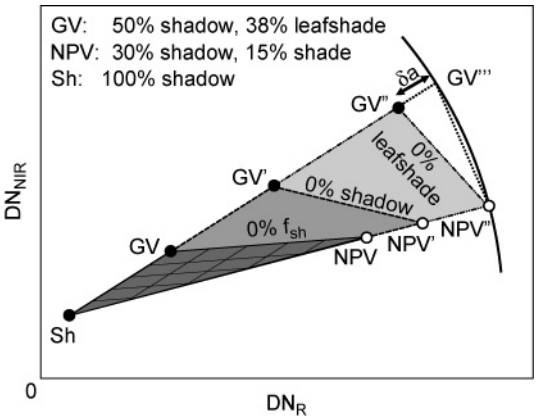

Figure 3 = Schematic mixing diagram for the ASTER channel 3 (NIR) vs. 2 (R) plane, illustrating calibration. Image-defined endmembers for shade, green vegetation, and non-photosynthetic vegetation are indicated by Sh, GV, and NPV. The mixing plane is shaded dark gray and shows isolines for f_{sh}=0 (no shade), 0.2, 0.4, 0.6, and 0.8; f_{sh}=1 (full shade) plots at Sh. Isolines for NPV (but not GV) are also shown. Shaded GV plots along the GV-Sh line; mixtures of GV and NPV plot along the f=0 line. Ternary mixtures of GV, NPV and Sh plot within the dark shaded triangle, and mixtures with less shade (f_{sh}<0) than the endmembers GV and NPV plot beyond the f_{sh}=0 isoline. After calibration of the f_{sh} image, positions of GV and NPV endmembers with no shadows can be plotted on their respective mixing lines with Sh (GV' & NPV'). For these points, leafshade is unchanged. Mixing now occurs in the (Sh, GV', NPV') triangle shaded intermediate gray, and the isolines for f_{sh} may be discordant with the ones in the (Sh, GV, NPV) triangle. All image data will now plot within the new triangle (no negative Sh fractions). Further extrapolation to GV'' and NPV'' gives virtual endmember positions assuming that leafshade is zero, as might occur looking directly down-sun (zero phase angle). However, GV and NPV may have different albedoes (here $a_{NPV} > a_{GV}$)

[1] Maryland Department of Natural Resources, Annapolis, Maryland: http://dnrweb.dnr.state.md.us/gis/data/lidar/

such that the vector Sh-GV'' is shorter than the vector Sh-NPV: the difference is a measure of the difference in albedo (δa), and GV''' is the position GV at zero phase-angle would have if $a_{NPV}=a_{GV}$. The arc shows the locus of a vector rotated about Sh.

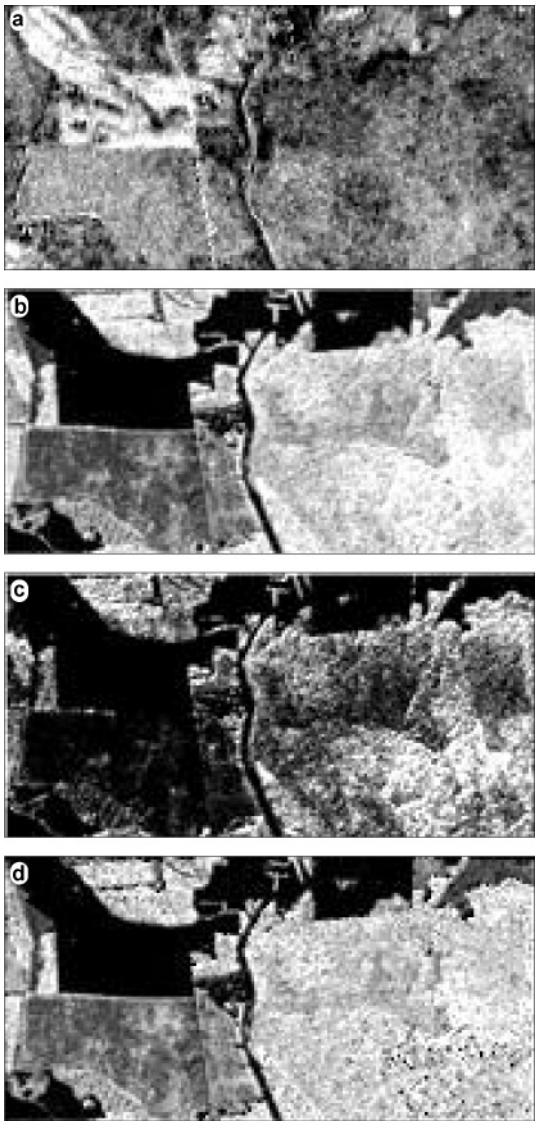

Figure 4. Individually stretched shade fraction images at 15-m resolutions: high-shade areas are light. a) ASTER Shade from SMA (f_{sh}). The rms value for the unmixing model was <0.5 DN, close to the precision level of the data. b) LiDAR treeshade (S+(1-S)·(1-cos(i)). c) LiDAR shadow (S). d) LiDAR shading (1-cos(i)). In calculating Λ, we assumed χ=1.

4 RESULTS AND DISCUSSION

The scattergram for f_{sh} *vs.* S (not shown) displays an overall lack of correlation, but for three forest sites within map unit 5, f_{sh} and S are linearly related. Calibration with these data yielded c_0 = -0.66, c_1 = 2.575, and Λ=0.77. These results allowed the quantitative comparison of ASTER and LiDAR data, shown in Figure 4. In particular, using equation 2 and calibrated f_{sh} and S images (Figs. 4a,c), we were able to calculate the leafshade (Λ) image shown in Figure 5. The Λ image has lower variability than its precursor images. It contains different information than f_{sh}, and appears to relate more directly to species and community type, whereas S is controlled strongly by stand age or structural stage. However, the strongest pattern appears to be related to unit boundaries between stands, with the 15-20 m trees appearing to have higher amounts of Λ than taller or shorter ones. Thus, Λ is not related strictly to canopy height. It will require field evaluation to sort this out, but we have not yet conducted a field validation of the Λ images.

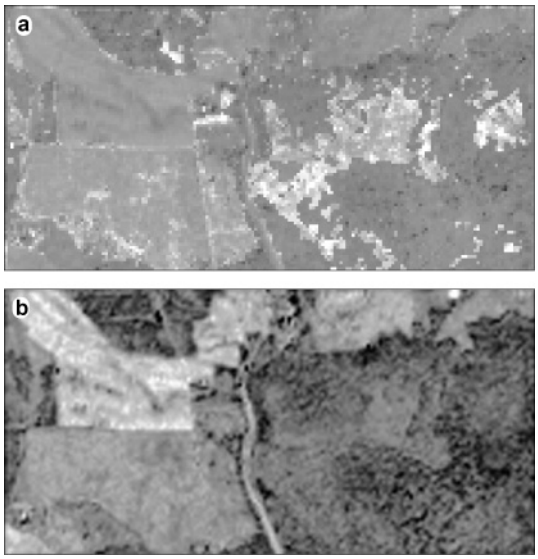

Figure 5. Leafshade Λ image. a) Calculated using eqn. 2. b) Approximated as f_{sh}/treeshade.

Figure 6b presents a simplified version of a Λ image. The variance is greater than for Figure 6a, probably because not as much treeshade was removed. This possibility is strengthened by the added detail in the tallest canopies which have the greatest potential for shadowing. However, calculation is simpler and such products may find practical application.

Hillshade correction was not addressed in this study, but is a common feature of forests and must be dealt with if parsing shade is to have practical use. *Gu and Gillespie* (1998) pointed out that in forests slopes

affected shadowing by uphill or downhill trees. However, slope also affects χ because shadows are near the principal plane, changing the shading integrated azimuthally. Because of this, it is unlikely that conventional Lambertian correction for slopes will be effective tool in isolating leafshade in hilly terrain.

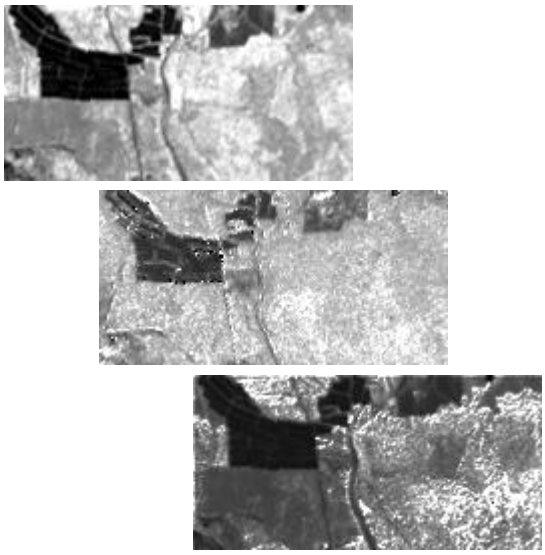

Figure 6. a) GV. b) GV/(1-f_{sh}). c) GV/(1-Treeshade).

Reduction of the albedo-*Sh* ambiguity was not addressed in this study, but is an important problem that must be dealt with to maximize the value of leafshade analysis. In the framework of this paper, it is grouped together with χ in Eqn 3 and cannot be separated. However, Figure 3 hints at the possibility of identifying relative albedo differences from endmember to endmember, with the possibility that knowing the albedo for a single endmember would suffice to determine albedo for all.

5 CONCLUSIONS

Remotely sensed spectral images integrate the effects of lighting up to the pixel scale. Blending contributions from topography, canopies, and leaves and branches. Hybrid analysis of spectral and LiDAR images can be used to separate contributions from shadows at the tree and stand scales from shading and shadowing at sub-tree scales, and spectral mixture models can be calibrated so that spectral shade fractions (f_{sh}) correspond to more direct measurements from LiDAR. For a deciduous forest in coastal Maryland, viewed in late morning during late spring, leafshade was typically ~0.7; treeshade was ~0.3-0.8. Future analysis is necessary to account for topographic shading and shadowing, to incorporate a more accurate photometric function χ, and to separate darkening due to albedo *a* on a pixel-by-pixel basis.

6 ACKNOWLEDGMENTS

Review by J. B. Adams improved the manuscript. Funding to UW personnel was through NGA Contract NMO715551/1252463 and NASA Contract NNG04HZ55C (ASTER).

7 REFERENCES

Adams, J. B., and Gillespie, A. R., 2006. *Remote Sensing of Landscapes with Spectral Images: A Physical Modeling Approach.* Cambridge University Press, Cambridge, UK, 362 pp.

Adams, J. B., Smith, M. O., and Johnson, P. E., 1986, Spectral mixture modeling: a new analysis of rock and soil types at the Viking Lander I site. *Journal of Geophysical Research* 91, 8098-8112.

Dymond, J., Shepherd, J. D., and Qi, J., 2001. A simple physical model of vegetation canopy reflectance. *Remote Sensing of Environment* 75, 35 -35.

Gu, D., and Gillespie, A. R., 1998. Topographic normalization of Landsat TM images of forests based on subpixel sun-canopy-sensor geometry. *Remote Sensing of Environment* 64, 166-175.

Franklin, J., Davis, F. W., and Lefebvre, P., 1991. Thematic Mapper analysis of tree cover in semiarid woodlands using a model of canopy shadowing, *Remote Sensing of Environmen*t 36, 189-202.

Hall, F. G., Knapp, D. E., and Huemmrich, K. F., 1997. Physically based classification and satellite mapping of biophysical characteristics in the southern boreal forest. *Journal of Geophysical Research* 102(D24), 29,567-29,580.

Kauth, R. J., and Thomas, G. S., 1976. The tasseled cap – a graphic description of the spectral temporal development of agricultural crops as seen by Landsat. Symposium Proceedings, Machine Processing of Remotely Sensed Data. Purdue University, IN, pp. 41-51.

Li, X., Strahler, A. H., and Woodcock, C. E., 1995. A hybrid geometric optical radiative transfer approach for modeling albedo and directional reflectance of discontinuous canopies. *IEEE Transcations on Geoscience and Remote Sensing* 33, 466-480.

Retzlaff, R., Gillespie, A., Weeks, R., and Haugerud, R., 2002. Parsing the Shade Fraction of a TM Image Using Lidar Data, Kitsap County, Washington (poster). American Society of Photogrammetry and Remote Sensing Conference, Seattle, WA, Fall.

Roberts, D.A., Adams, J.B., and Smith, M.O., 1993. Discriminating Green Vegetation, Non-Photosynthetic Vegetation and Soils in AVIRIS Data. *Remote Sensing of Environment* 44(2/3), 255-270.

Sabol, D. E., Jr., Gillespie, A. R., Adams, J. B., Smith, M. O., and Tucker, C. J., 2002. Structural stage in Pacific Northwest forests estimated using simple mixing models of multispectral images. *Remote Sensing of Environment* 80(1), 1-16.

Strahler, A., 1997. Vegetation canopy reflectance modeling - Recent developments and remote sensing perspectives. *Remote Sensing Reviews* 15, 179-194.

Verhoef, W., 1984. Light scattering by leaf layers with application to canopy reflectance modeling: The SAIL method. *Remote Sensing of Environment* 16, 125-141.